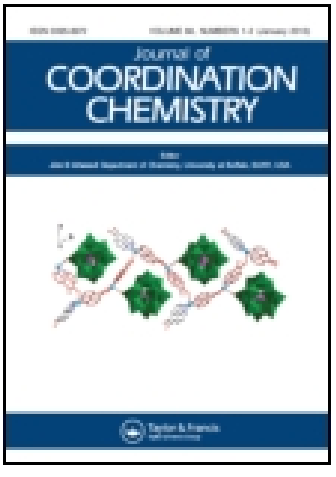

Journal of Coordination Chemistry
Publication details, including instructions for authors and subscription information:
http://www.tandfonline.com/loi/gcoo20

Four diclofenac complexes with cobalt(II) and nickel(II) ions: synthesis, spectroscopic properties, thermal decompositions, crystal structures, and carbonic anhydrase activities

Sema Caglar[a], Ismihan E. Aydemir[a], Murat Cankaya[b], Mehmet Kuzucu[b], Ersin Temel[c] & Orhan Buyukgungor[c]

[a] Faculty of Arts and Sciences, Department of Chemistry, Erzincan University, Erzincan, Turkey

[b] Faculty of Arts and Sciences, Department of Biology, Erzincan University, Erzincan, Turkey

[c] Faculty of Arts and Sciences, Department of Physics, Ondokuz Mayis University, Samsun, Turkey

Accepted author version posted online: 12 Mar 2014.Published online: 04 Apr 2014.

To cite this article: Sema Caglar, Ismihan E. Aydemir, Murat Cankaya, Mehmet Kuzucu, Ersin Temel & Orhan Buyukgungor (2014) Four diclofenac complexes with cobalt(II) and nickel(II) ions: synthesis, spectroscopic properties, thermal decompositions, crystal structures, and carbonic anhydrase activities, Journal of Coordination Chemistry, 67:6, 969-985, DOI: 10.1080/00958972.2014.903327

To link to this article: http://dx.doi.org/10.1080/00958972.2014.903327

Journal of Coordination Chemistry, 2014
Vol. 67, No. 6, 969–985, http://dx.doi.org/10.1080/00958972.2014.903327

Four diclofenac complexes with cobalt(II) and nickel(II) ions: synthesis, spectroscopic properties, thermal decompositions, crystal structures, and carbonic anhydrase activities

SEMA CAGLAR*†, ISMIHAN E. AYDEMIR†, MURAT CANKAYA‡, MEHMET KUZUCU‡, ERSIN TEMEL§ and ORHAN BUYUKGUNGOR§

†Faculty of Arts and Sciences, Department of Chemistry, Erzincan University, Erzincan, Turkey
‡Faculty of Arts and Sciences, Department of Biology, Erzincan University, Erzincan, Turkey
§Faculty of Arts and Sciences, Department of Physics, Ondokuz Mayis University, Samsun, Turkey

(*Received 21 October 2013; accepted 18 February 2014*)

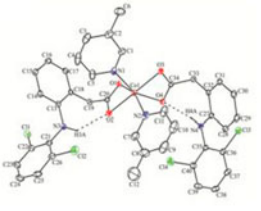

$[Co(dicl)_2(3\text{-}pic)_2]$

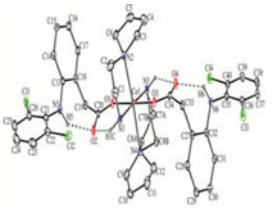

$[Co(dicl)_2(2\text{-}aepyr)_2]$

Cobalt(II) and nickel(II) complexes with diclofenac (dicl) in the presence of nitrogen-donor 3-picoline (3-pic) and 1-(2-aminoethyl)pyrrolidine (2-aepyr), $[Co(dicl)_2(3\text{-}pic)_2]$ (**1**), $[Ni(dicl)_2(3\text{-}pic)_2(H_2O)_2]$ (**2**), $[Co(dicl)_2(2\text{-}aepyr)_2]$ (**3**), and $[Ni(dicl)_2(2\text{-}aepyr)_2]$ (**4**), have been synthesized and characterized by FT-IR, UV–Vis, elemental and thermal analysis. The crystal structures of **1** and **3** have been determined by single-crystal X-ray diffraction; phase purity of complexes has been proved by powder X-ray diffraction analysis. Structural analyses have demonstrated that **1** and **3** are mononuclear and Co(II) ions have distorted octahedral environments. In **1**, dicl is bidentate, whereas in **2**, **3**, and **4** dicl is monodentate. Dicl ligands are coordinated to metal(II) ions with O of carboxylate. Therefore, IR spectra of all complexes display $\{\nu(OCO)_{asym}$ and $\nu(OCO)_{sym}\}$ of dicl. The calculated $\Delta\nu(OCO)$ values are consistent with the presence of monodentate (>200) and bidentate (<200) carboxylate. Compounds **2**, **3**, and **4** exhibit inhibition effects on human carbonic anhydrase-I. Compounds **3** and **4** show high thermal stability compared with **1** and **2**.

Keywords: Diclofenac; Carbonic anhydrase; Nonsteroidal anti-inflammatory drugs; Crystal structure

1. Introduction

Nonsteroidal anti-inflammatory drugs (NSAIDs) are commonly used as analgesic, anti-inflammatory, antipyretic agents and are among the most used medical drugs [1]. NSAIDs consist of salicylate derivatives, phenylalkanoic acids, oxicams, anthranilic acids,

*Corresponding author. Email: scaglar@erzincan.edu.tr

sulfonamides, and furanones [2]. Diclofenac (dicl), alternatively named 2-(2,6-dicholoroanilino)phenylacetic acid, is a part of the NSAIDs group of phenylalkanoic acids. Dicl, in the form of its water soluble sodium salt, is widely used as analgesic, anti-inflammatory, and antipyretic agents [3–9]. It is used in sport injuries, painful, and inflammation conditions. These drugs exhibit an inhibition or activation effect on organism or cells. These effects are very important to continuation of organism's life. Organisms contain many vital enzymes consisting of single or family. Carbonic anhydrase (CA) family controls a crucial biological function. This family catalyzes the conversion of CO_2 and H_2CO_3 in cells and intercellular fluid. The reaction of CA catalyzes is essential to physiological processes such as calcification, photosynthesis, respiration, ionic, acid–base, and fluid balance, metabolism, and cell growth [10, 11]. CA-I is the cytosolic form of CA isoforms, present in erythrocytes [12, 13]. Therefore, investigations of inhibition effects of drugs on this CA isoform are crucial for life.

Many spectroscopic and non-spectroscopic techniques were used to explain the sodium diclofenac (Nadicl) structure. The techniques are as follows: FT-IR [14, 15], calorimetry [16–18], UV–Vis spectroscopy [19], gas [20, 21] and liquid chromatography [22, 23] and NMR spectroscopy [24]. The crystal structures of nickel(II), copper(II), cadmium(II), and tin(IV) complexes with dicl ligands have been determined [4, 14, 25–28]. Compared with Cu(II) analogs, nickel(II)-dicl complex displayed more biological activity than the parent drugs [4]. Dicl is a polyfunctional ligand, due to the presence of the negatively charged carboxylate oxygens.

In the present study, we have focused on the coordination chemistry of dicl with metal ions in an attempt to examine their mode of binding and inhibitory effects on human blood carbonic anhydrase I (hCA-I) of the complexes. Here, we report the synthesis, spectral, thermal characterizations, crystal structures, and inhibitory effects of neutral cobalt(II) and nickel(II) complexes with dicl in the presence of aromatic 3-picoline (3-pic) and nonaromatic 1-(2-aminoethyl)pyrrolidine (2-aepyr).

2. Experimental setup

2.1. *Methods of sample characterization*

$CoCl_2 \cdot 6H_2O$ (Sigma), $Ni(NO_3)_2 \cdot 6H_2O$ (Sigma), $NiCl_2 \cdot 6H_2O$ (Sigma), sodium diclofenac (Sigma, 99.00%), 3-picoline (Aldrich, 99.00%), and 1-(2-aminoethyl)pyrrolidine (Aldrich, 98.00%) were used for preparation of the complexes. Infrared spectra of the complexes were recorded with a Thermo Nicolet 6700 spectrophotometer from 4000 to 450 cm^{-1} at a resolution of 4 cm^{-1} using KBr pellets. UV–Vis spectra were recorded on a PG 80+ from 200 to 1100 nm in methanol. C, H, and N elemental analyses were performed on a LECO CHNS-932 elemental analyzer. The TG and DTA curves were scanned using a PRIS Diamond TG/DTG apparatus in air (heating rate: 10 °C min^{-1}, platinum crucibles, mass ~10 mg from 30 to 1000 °C). The powder X-ray diffraction (PXRD) patterns of complexes were taken at ambient temperatures by the use of a PANalytical Empyrean diffractometer using Ni filtered CuK_α radiation ($\lambda = 1.54050$ Å; 45 kV, and 40 mA). The theoretical PXRD patterns were simulated from single-crystal data using PLATON [29].

2.2. *Synthesis of [Co(dicl)$_2$(3-pic)$_2$] (1)*

$CoCl_2 \cdot 6H_2O$ (0.06 g, 0.3 mM) and Nadicl (sodium diclofenac) (0.18 g, 0.6 mM) were dissolved in ethanol (40 cm^3) with continuous stirring at 50 °C. Then, 3-pic (98 µL, 0.6 mM) was added.

The resulting solution was allowed to evaporate slowly at room temperature and X-ray quality purple crystals appeared after a few days. Yield: 80%; Analytical data for [$C_{40}H_{34}N_4O_4Cl_4Co$]: Found: C, 57.50; H, 4.10; N, 6.72%; Calcd: C, 57.62; H, 4.07; N, 6.70%.

2.3. *Synthesis of [Ni(dicl)$_2$(3-pic)$_2$(H$_2$O)$_2$] (2)*

$Ni(NO_3)_2 \cdot 6H_2O$ (0.06 g, 0.3 mM) and Nadicl (0.18 g, 0.6 mM) were dissolved in methanol (40 cm^3) with continuous stirring at 50 °C. Then, 3-pic (98 µL, 0.6 mM) was added. The resulting solution was allowed to evaporate slowly at room temperature and green microcrystals appeared after one week. Yield: 75%; Analytical data for [$C_{40}H_{38}N_4O_6Cl_4Ni$]: Found: C, 55.12; H, 4.21; N, 6.51%; Calcd: C, 55.08; H, 4.36; N, 6.43%.

2.4. *Synthesis of [Co(dicl)$_2$(2-aepyr)$_2$] (3)*

$CoCl_2 \cdot 6H_2O$ (0.06 g, 0.3 mM) and Nadicl (0.18 g, 0.6 mM) were dissolved in ethanol (40 cm^3) with continuous stirring at 50 °C. Then 2-aepyr (0.07 g, 0.6 mM) was added. The resulting solution was allowed to evaporate slowly at room temperature and X-ray quality pink crystals appeared after two weeks. Yield: 65%; Analytical data for [$C_{40}H_{48}N_6O_4Cl_4Co$]: Found: C, 55.12; H, 5.48; N, 9.72%; Calcd: C, 54.69; H, 5.46; N, 9.57%.

2.5. *Synthesis of [Ni(dicl)$_2$(2-aepyr)$_2$] (4)*

Complex **4** was prepared in a similar way to **3** with the use of $NiCl_2 \cdot 6H_2O$. The resulting solution was allowed to evaporate slowly at room temperature and blue microcrystals appeared after one month. Yield: 86%; Analytical data for [$C_{40}H_{48}N_6O_4Cl_4Ni$]: Found: C, 54.80; H, 5.38; N, 9.61 %; Calcd: C, 54.69; H, 5.46; N, 9.57%.

2.6. *X-ray crystallography*

The diffraction data were collected on a STOE IPDSII image plate detector using Mo Kα radiation ($\alpha = 0.71073$ Å, $T = 293$ K). A summary of the key crystallographic information is given in table 1. Data collection: Stoe X-AREA [30]. Cell refinement: Stoe X-AREA [30]. Data reduction: Stoe X-RED [30]. The structure was solved by direct-methods using SHELXS-97 [31] and anisotropic displacement parameters were applied to non-hydrogen atoms in a full-matrix least-squares refinement based on F^2 using SHELXL-97 [31]. All hydrogens attached to carbon were positioned geometrically and refined by a riding model with Uiso 1.2 times that of the attached atom; the remaining hydrogens were located from the Fourier difference map.

2.7. *Purification of CA isoenzymes from human blood by affinity chromatography*

The purification of hCA-I isoenzyme from human blood erythrocytes was performed in a simple single-step method by Sepharose-4B-L tyrosine-sulfanilamide affinity gel chromatography. Erythrocytes were purified from fresh human blood obtained from the Blood Center of Erzincan State Hospital. Purification methods of CA-I were carried out as previously described [32, 33].

Table 1. Crystal data and structure refinement parameters for **1** and **3**.

	1	**3**
Empirical formula	$C_{40}H_{34}N_4O_4CI_4Co$	$C_{40}H_{48}N_6O_4CI_4Co$
Formula weight	835.44	877.57
Temperature (K)	293	293
Wavelength (Å)	0.71073	0.71073
Crystal system	Triclinic	Monoclinic
Space group	*P-1*	*P 21/c*
Unit cell dimensions		
a (Å)	11.3968 (6)	12.9980 (3)
b (Å)	12.0094 (7)	14.6148 (4)
c (Å)	15.3049 (9)	22.0893 (5)
α (°)	85.341 (5)	90.00
β (°)	69.477 (4)	104.946 (2)
γ (°)	82.048 (5)	90.00
V (Å)^3	1941.74 (19)	4054.19 (17)
Z	2	4
A coefficient (mm^{-1})	0.763	0.736
D_{Calcd} (mg m^{-3})	1.429	1.438
Crystal size (mm)	0.46; 0.53; 0.58	0.11; 0.24; 0.49
Theta range for data collection (°)	1.92; 28.06	1.39; 27.30
Measured reflections	19,762	49,580
Independent reflections	8038	8412
Absorption correction	Integration[a]	Integration[a]
Refinement method	Full-matrix least-squares on F^2	Full-matrix least-squares on F^2
Final *R* indices [$F^2 > 2\ \sigma(F^2)$]	0.0623	0.0841
Goodness-of-fit on F^2	1.047	1.041
Largest diff. peak and hole (e/Å^3)	−0.445; 1.437	−0.48; 0.878

[a]Stoe and Cie (2002) [31].

2.7.1. Hydratase activity assay. CA activity was assayed by following the hydration of CO_2 according to the method described by Ayvaz *et al.* [34]. CO_2-hydratase activity as an enzyme unit (EU) was calculated by using the equation (to − tc/tc) where to and tc are the times for pH change of the non-enzymatic and the enzymatic reactions, respectively.

2.7.2. Esterase activity assay. CA-I activity was determined by following the change in absorbance at 348 nm of 4-nitrophenylacetate (NPA) to 4-nitrophenylate ion over a period of 3 min at 25 °C using a spectrophotometer according to the method described by Verpoorte *et al.* [35]. The inhibitory effects of $[Co(dicl)_2(3\text{-pic})_2]$, $[Ni(dicl)_2(3\text{-pic})_2(H_2O)_2]$, $[Co(dicl)_2(2\text{-aepyr})_2]$, and $[Ni(dicl)_2(2\text{-aepyr})_2]$ were examined. All compounds were tested in triplicate at each concentration used. Different inhibitor concentrations were used. HCA-I enzyme activities were measured for $[Co(dicl)_2(3\text{-pic})_2]$ (0.001–1000 mM), $[Ni(dicl)_2(3\text{-pic})_2(H_2O)_2]$ (0.179–0.299 mM), $[Co(dicl)_2(2\text{-aepyr})_2]$ (0.342–0.456 mM), and $[Ni(dicl)_2(2\text{-aepyr})_2]$ (0.171–0.285 mM) at cuvette concentrations. Control cuvette activity in the absence of inhibitor was taken as 100%. For each inhibitor, activity (%)–[Inhibitor] graphs were drawn. To determine K_i values, three different inhibitor concentrations were tested. In these experiments, NPA was used as substrate at five different concentrations (0.15–0.75 mM), and Lineweaver–Burk curves were drawn [36].

2.7.3. Protein determination. Protein during the purification steps was determined spectrophotometrically at 595 nm according to the Bradford method [37].

Figure 1. Sodium dodecyl sulfate-polyacrylamide gel electrophoresis (SDS-PAGE) bands of carbonic anhydrase (hCA-I) purified from human blood. Column a: standard proteins, 1: MBP–paramyosin (fusion of MBP and paramyosin, 80 kDa); 2: MBP–chitin binding domain (CBD) (fusion of MBP and CBD, 58 kDa); 3: soybean trypsin inhibitor, 24 kDa). Column b: purified hCA-I.

2.7.4. SDS polyacrylamide gel electrophoresis. SDS polyacrylamide gel electrophoresis was performed after purification of the cord blood isoenzymes. It was carried out according to the Laemmli procedure [38]. The electrophoretic pattern was photographed (figure 1).

3. Results and discussion

The four diclofenac complexes were synthesized and characterized using FT-IR, UV–Vis, and elemental and thermal analysis techniques. The crystal structures of $[Co(dicl)_2(3\text{-pic})_2]$ and $[Co(dicl)_2(2\text{-aepyr})_2]$ were determined via single-crystal X-ray diffraction. Selected geometrical parameters for **1** and **3** are listed in table 1. The phase purity of complexes was confirmed by elemental analysis data and PXRD analysis. Based on the experimental data, $[Ni(dicl)_2(2\text{-aepyr})_2]$ is expected to be structurally similar to $[Co(dicl)_2(2\text{-aepyr})_2]$. Thermal analysis and FT-IR spectroscopic techniques show that **2** includes two water ligands, $[Ni(dicl)_2(3\text{-pic})_2(H_2O)_2]$, different from $[Co(dicl)_2(3\text{-pic})_2]$.

3.1. *Description of the crystal structure*

3.1.1. $[Co(dicl)_2(3\text{-pic})_2]$ (1). An ORTEP view of **1** with the atom numbering scheme is presented in figure 2. Selected bond distances and angles are given in table 2. Single-crystal X-ray analysis reveals that $[Co(dicl)_2(3\text{-pic})_2]$ is neutral and crystallizes in the triclinic space group *P-1*. Co(II) is coordinated by 3-pic as a monodentate donor via nitrogen and four carboxyl oxygens from two dicl ligands in octahedral geometry. Dicl is a bidentate ligand. The bond angles around cobalt(II) indicate a distortion from ideal octahedral geometry, especially observed in the bite angles O2–Co1–N1 with the values of 98.24(11)°, O1–Co1–O2 with values of 61.02(7)°, O3–Co1–O4, and O2–Co1–O4 with the values of 61.02(7)° and 108.03(8)°, respectively.

$Co–N_{3\text{-pic}}$ bond distances are 2.106(3)–2.131(3) Å, similar with corresponding values in $[Co(bba)_2(H_2O)_2(3\text{-pic})_2]$ (2.15(5) Å) [39], $[Co\{S_2P(OC_6H_4Me\text{-}p)_2\}_2(NC_5H_4Me\text{-}3)_2]$ (2.1755(3) Å) [40], $[Co\{S_2P(OC_6H_4Me\text{-}p)_2\}_2(C_5H_5N)_2]$ (2.162(2) Å) [41], and $[Co\{S_2P(OEt)_2\}_2(C_5H_5N)_2]$ (2.164(3) Å) [42], where bba, $S_2P(OC_6H_4Me\text{-}p)_2$, and NC_5H_4Me-3 are 2-benzoylbenzoate, bis(O,O°-ditolyl/dibenzyl/diphenyldithiophosphato), and 3-picoline. $Co\text{-}N_{3\text{-pic}}$ bond distances are slightly longer than the 2.046(2) Å found in $[Co(3\text{-pic})_2Cl_2]$ [43].

In the present structure, intramolecular N3–H3A···O2 and N4–H4A···O4 hydrogen bonds generates S(7) ring motives [44]. In addition to those, while intermolecular C33–H33B···$Cl1^{i}$ (i: $1-x$, $1-y$, $1-z$) hydrogen bonds generate $R_2^2(28)$ ring motives, the combination of the C33-H33B···$Cl1^{i}$ and C38–H38···$O1^{ii}$ (ii: x, $-1+y$, z) hydrogen bonds generate $R_4^4(38)$ ring motives. These adjacent motives are parallel to the *b*-axis (figure 3). The packing pattern generated by hydrogen bonds can be expressed as G(*n*) form using graph set notation. G is denoted by S (self) character for the ring generated by intramolecular hydrogen bonds while if the ring is formed by intermolecular hydrogen bonds, G is expressed by R (ring) letter. The terms *a*, *d*, and *n* refer to the number of acceptors (a), donors (d), and atom numbers in the motif.

3.1.2. $[Co(dicl)_2(2\text{-aepyr})_2]$ (3). The ORTEP view of the asymmetric unit of **3**, along with the atomic numbering scheme, is shown in figure 4. Selected bond lengths and angles of

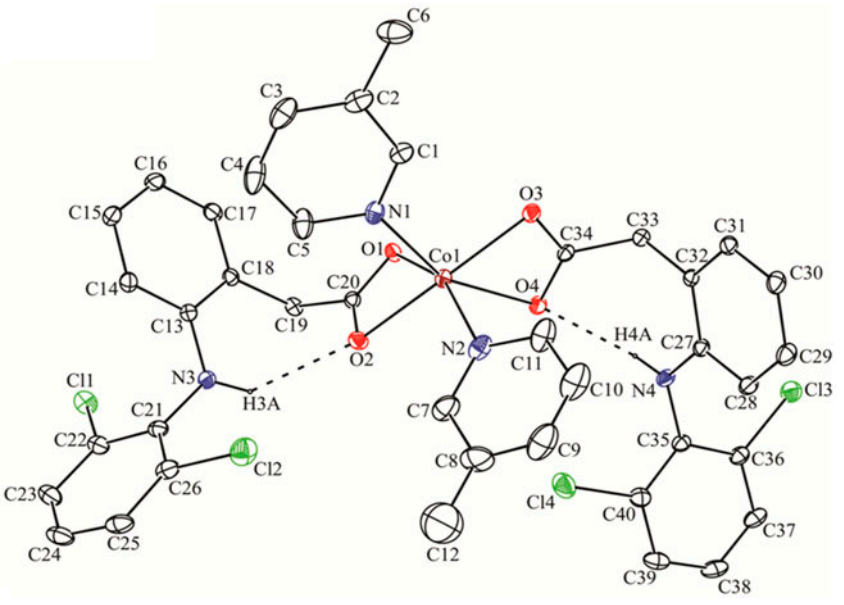

Figure 2. ORTEP III diagram and atom numbering scheme of **1**. Displacement ellipsoids are drawn at the 20% probability level.

Table 2. Selected bond distances (Å) and angles (°) for **1** and **3**.

1			
Co1–O1	2.1217 (19)	Co1–O4	2.228 (2)
Co1–O2	2.152 (2)	Co1–N1	2.131 (2)
Co1–O3	2.080 (2)	Co1–N2	2.106 (3)
O3–Co1–O1	103.34 (8)	N2–Co1–O2	97.00 (12)
O3–Co1–N2	96.42 (12)	O1–Co1–O2	61.02 (7)
N2–Co1–O1	155.88 (12)	N1–Co1–O2	94.03 (9)
O3–Co1–N1	95.75 (9)	O3–Co1–O4	60.52 (7)
N2–Co1–N1	98.24 (11)	N2–Co1–O4	88.48 (10)
O1–Co1–N1	93.45 (9)	O1–Co1–O4	89.32 (7)
O3–Co1–O2	162.07 (9)	N1–Co1–O4	156.03 (9)
O2–Co1–O4	108.03 (8)		
3			
Co1–O1	2.095 (2)	Co1–N2	2.349 (3)
Co1–O3	2.077 (2)	Co1–N3	2.111 (3)
Co1–N1	2.116 (3)	Co1–N4	2.322 (3)
O3–Co1–O1	178.34 (10)	N3–Co1–N4	81.05 (11)
O3–Co1–N3	92.60 (11)	N1–Co1–N4	97.22 (11)
O1–Co1–N3	88.35 (11)	O3–Co1–N2	89.97 (11)
O3–Co1–N1	84.39 (11)	O1–Co1–N2	88.50 (11)
O1–Co1–N1	94.71 (11)	N3–Co1–N2	102.29 (12)
N3–Co1–N1	176.48 (12)	N1–Co1–N2	79.57 (12)
O3–Co1–N4	92.02 (11)	N4–Co1–N2	176.04 (11)
O1–Co1–N4	89.47 (11)		

the Co(II) complex are given in table 2. Complex **3** crystallizes in the monoclinic space group *P 21/c*. Cobalt(II) exhibits a slightly distorted octahedral coordination geometry of four nitrogens from two 2-aepyr and two dicl ligands. The extent of deviation from an octahedral geometry varies from 0.3° to 8.95° from the ideal value of 90°.

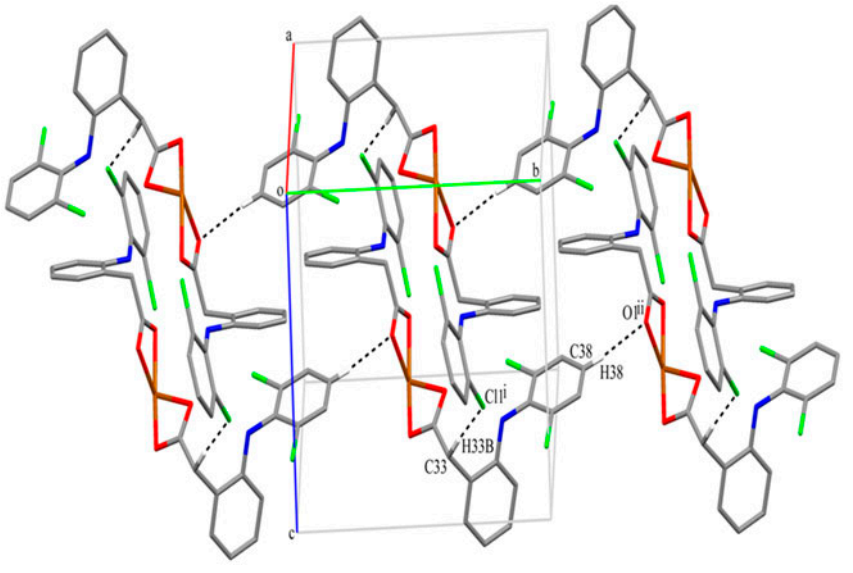

Figure 3. The molecular packing of **1** showing the formation of $R_2^2(28)$ and $R_4^4(38)$ ring motives. The methyl pyridine moieties have been omitted for clarity. Symmetry codes: (i) $1-x, 1-y, 1-z$; (ii) $x, -1+y, z$.

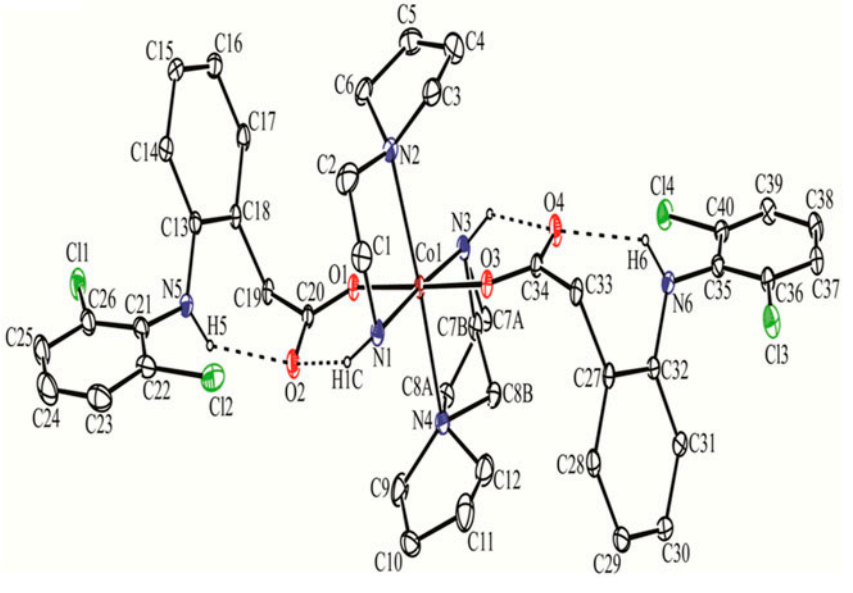

Figure 4. ORTEP III diagram and atom numbering scheme of **3**. Displacement ellipsoids are drawn at the 20% probability level.

The ethyl group (C7–C8 atoms) of 2-aepyr shows disorder. The hydrogen bonding geometries are given in table 3.

Intramolecular N–H···O hydrogen bonds between N–H group of 2-aepyr and carboxyl oxygen of dicl and also between the N–H group of dicl and carboxyl oxygen of dicl occur.

Table 3. Hydrogen-bonding geometries for **1** and **3** (Å, °).

D–H···*A*	*D*–H	H···*A*	*D*···*A*	*D*–H···*A*
1				
N3–H3A···O2	0.86	2.31	2.987(3)	135.5
N4–H4A···O4	0.86	2.27	2.879(3)	127.8
C33–H33B···Cl1^{i}	0.97	2.75	3.710(3)	173
C38–H38···O1^{ii}	0.93	2.59	3.495(5)	163
C24–H24···O1^{iii}	0.93	2.56	3.290(6)	135
3				
N1–H1C···O2	0.90	2.07	2.830(4)	141.3
N3–H3D···O4	0.90	2.23	2.916(4)	133.1
N5–H5···O2	0.86	2.11	2.825(4)	139.6
N6–H6···O4	0.86	2.27	2.937(4)	134
N1–H1D···Cl4^{i}	0.90	2.93	3.767(3)	155.3
N3–H3C···Cl3^{ii}	0.90	2.89	3.639(3)	141.3

1 i: $1-x$, $1-y$, $1-z$; ii: $-1+x$, y, z; iii: x, $-1+y$, z; **3** i: $-x+2$, $y-1/2$, $-z+3/2$; ii: $-x+2$, $y+1/2$, $-z+3/2$.

Intramolecular N1–H1C···O2 and N3–H3D···O4 hydrogen bonds generate S(6) ring motives while N5–H5···O2 and N6–H6···O4 hydrogen bonds generate S(7) ring motives [44]. Adjacent complex units are connected via intermolecular N–H···Cl hydrogen bond between the N–H group of 2-aepyr ligand and chloro atom of dicl ligand. Intermolecular N1–H1D···Cl4^{i} (i: $-x+2$, $y-1/2$, $-z+3/2$) and N3–H3C···Cl3^{ii} (ii: $-x+2$, $y+1/2$, $-z+3/2$) hydrogen bonds generate adjacent $R_2^2(24)$ ring motives (figure 5).

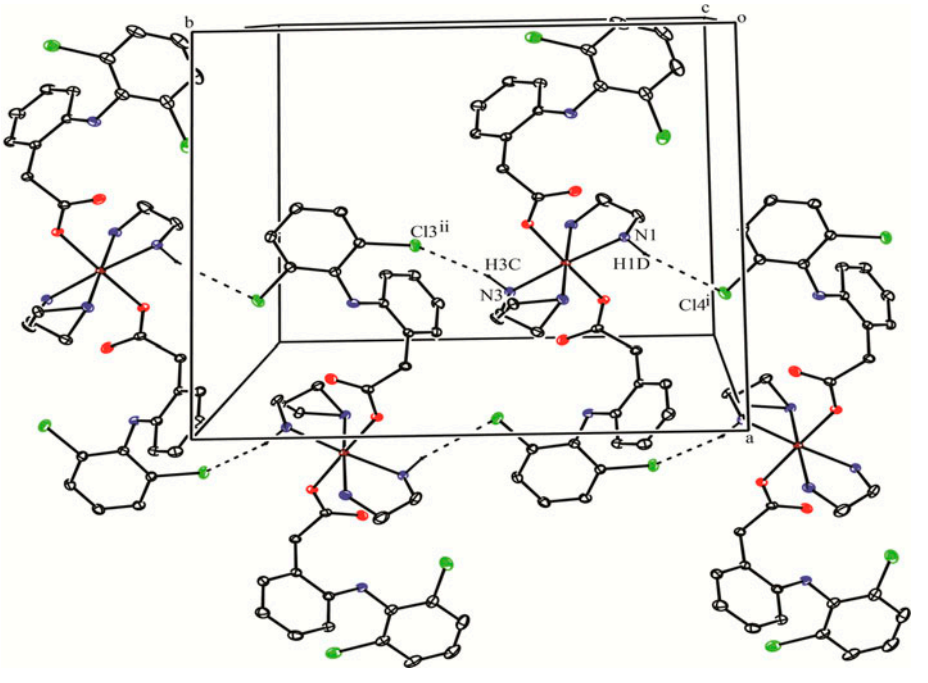

Figure 5. The molecular packing of **3** showing formation of $R_2^2(24)$ ring motives. The pyrrolidine moieties have been omitted for clarity. Symmetry codes: (i) $-x+2$, $y-1/2$, $-z+3/2$; (ii) $-x+2$, $y+1/2$, $-z+3/2$.

3.2. *Powder X-ray diffraction*

PXRD was performed on the metal complexes (figure 6). The PXRD patterns of the complexes demonstrated sharp intense peaks indicating their crystalline phase. The experimental PXRD patterns of **1** and **3** closely match simulations obtained from the appropriate single XRD measurements, confirming phase purity of the products [45]. However, some small differences were observed in the intensities of reflections. The differences in intensity may be due to preferred orientation of crystallites in powder samples [45]. Comparison of simulated and experimental PXRD patterns of **1** and **3** is given in figures 7 and 8, respectively.

3.3. *IR spectra*

The band assignments of Nadicl and complexes are listed in table 4. ν(NH) of a secondary amino group of Nadicl is observed at 3250 cm^{-1}. In complexes, this band is at 3236, 3232, 3198, and 3201 cm^{-1}, respectively. The band at 3347 cm^{-1} for **3** and 3353 cm^{-1} for **4** could be ascribed to stretch of N–H, suggesting the presence of amino group of 1-(2-aminoethyl) pyrrolidine. A broad functional group region indicates that water participated in the coordination in **2**. The band at 3304 cm^{-1} corresponds to the O–H stretch of water. The asymmetric and symmetric stretching peaks of both aromatic and aliphatic ν(CH) bonds of Nadicl, 3-picoline and 1-(2-aminoethyl)pyrrolidine are at 3063–2832 cm^{-1}. The $\nu_{asym}(COO^-)$ of free Nadicl at 1572 cm^{-1} shifts to 1548, 1579, 1577, and 1577 cm^{-1} for complexes, $\nu_{sym}(COO^-)$ at 1399 cm^{-1} shifts in complexes to 1418, 1379, 1368, and 1368 cm^{-1}, respectively. The difference $\Delta\nu$ [$\nu_{asym}(COO) - \nu_{sym}(COO)$], a useful tool for determining the coordination mode of carboxylate ligands, is calculated as 130, 200, 209, and 209 cm^{-1}, respectively, bidentate

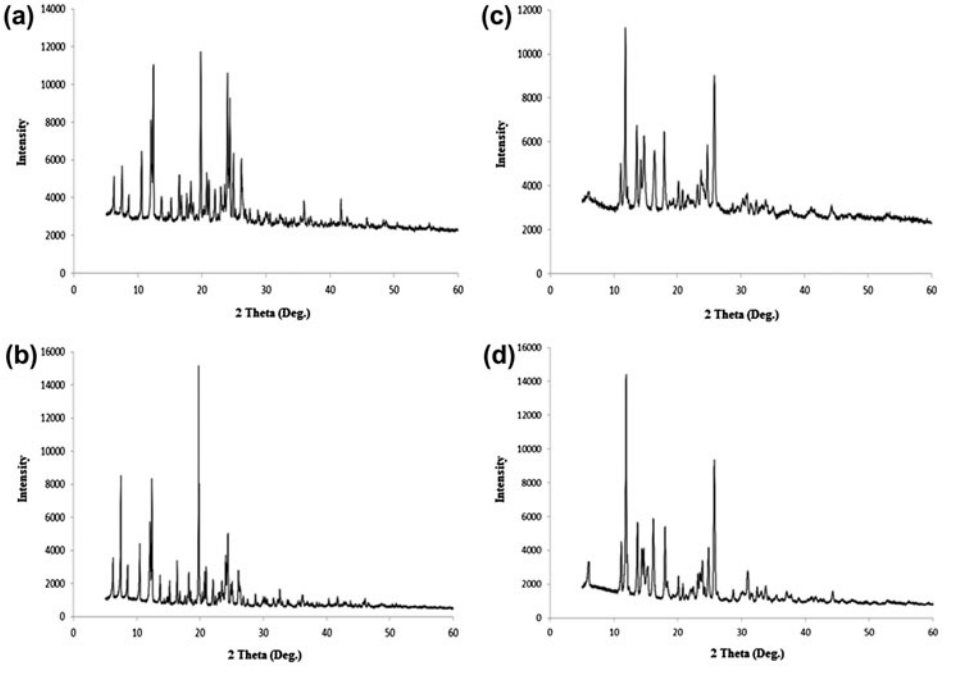

Figure 6. PXRD patterns for (a) **1**, (b) **2**, (c) **3**, and (d) **4**.

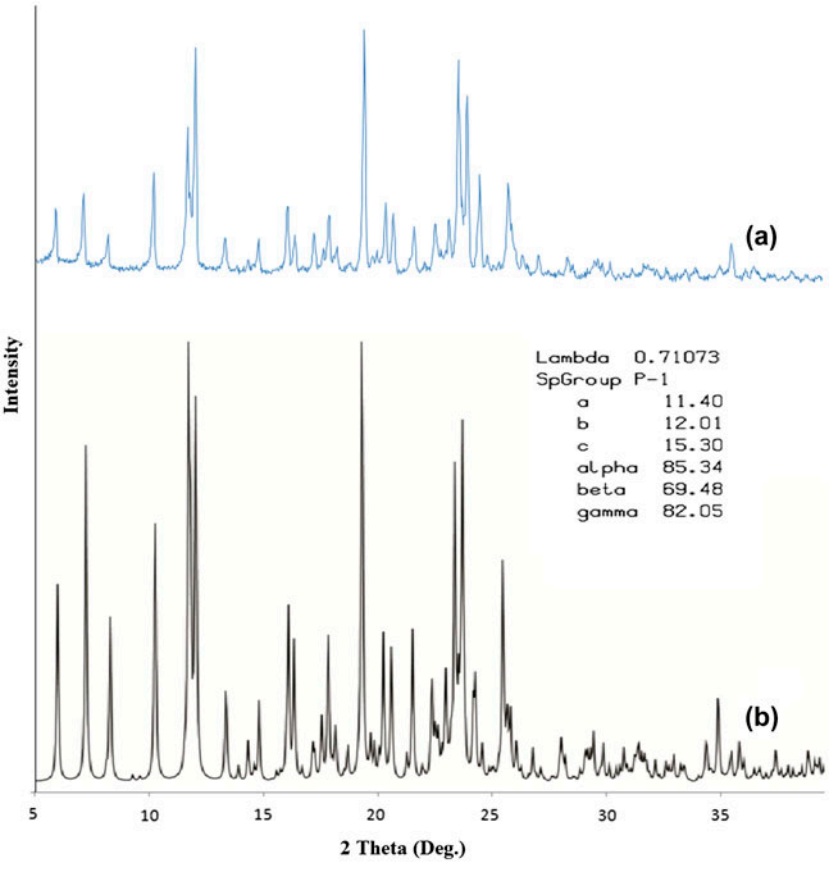

Figure 7. Experimental (a) and simulated (b) PXRD patterns for **1**.

(<200 cm^{-1}) coordination for **1**; monodentate (>200 cm^{-1}) coordination for **2**, **3**, and **4** [46]. Bands at 1613–1604 cm^{-1} arise from phenyl ring stretching vibrations of Nadicl and other ligands. Medium intensity bands at 1312–1309 cm^{-1} may be assigned to ν(C–N–C) asymmetric stretch while weak bands at 1239 cm^{-1} are assigned to ν(C–N–C) symmetric stretch of Nadicl. The band attributed to in plane deformation vibration of the ν(CH) occurs at 940 cm^{-1}. Bands at 760 cm^{-1} correspond to ν(C–Cl) of Nadicl. The band under 600 cm^{-1} in complexes may be attributed to metal–oxygen and metal–nitrogen stretches.

3.4. *UV–Vis spectra*

The electronic absorption spectra of **1–4** were recorded at room temperature in methanol. Each complex shows an absorption lower than 370 nm due to intramolecular $\pi \rightarrow \pi^*$ and $n \rightarrow \pi^*$ transitions for the aromatic ring. The absorption spectrum of **1** has three bands, the band at 980 nm may be attributed to a $^4T_{1g}(F) \rightarrow {}^4T_{2g}(F)$ transition, a band exists at 468 nm ($\varepsilon = 18\ dm^3\ M^{-1}\ cm^{-1}$) due to d–d transition from a $^4T_{1g}(F) \rightarrow {}^4A_{2g}(F)$, and the third band at 390 nm may be attributed to a $^4T_{1g}(F) \rightarrow {}^4T_{1g}(P)$ transition. Complex **3** in the visible region has two low intensity bands assigned to d–d transitions. These bands at 540 nm

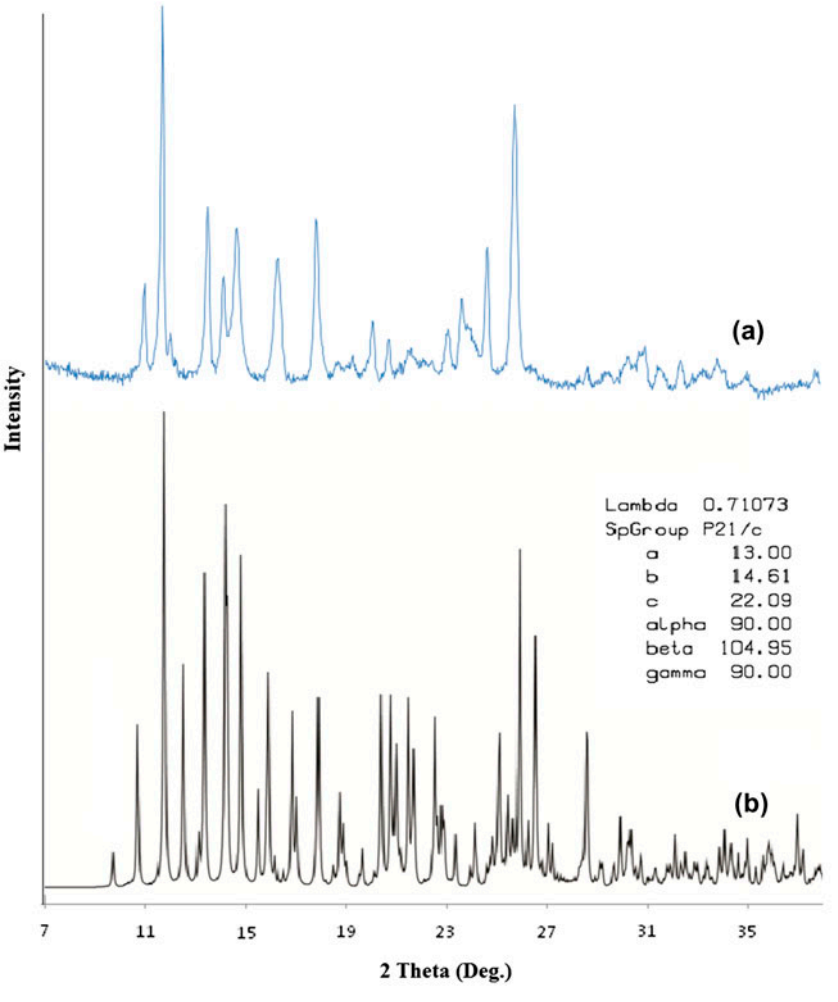

Figure 8. Experimental (a) and simulated (b) PXRD patterns for **3**.

Table 4. Selected IR spectral data[a] for dicl, **1**, **2**, **3**, and **4**.

	dicl	**1**	**2**	**3**	**4**
$\nu(NH)_{dicl}$	3250m	3236m	3232m	3198m	3201m
$\nu(NH)_{2\text{-aepyr}}$	–	–	–	3347m	3353m
$\nu(OH)$	–	–	3304b,m	–	–
$\nu_{aro}(CH)$	3060w	3010w	3063w	3015w	3045w
$\nu_{alf}(CH)$	2980w	2854w	2813w	2974–2832m	2974–2838m
$\nu_{asym}(COO^-)$	1572s	1548s	1577s	1577s	1577s
$\nu_{sym}(COO^-)$	1399w	1418w	1385w	1368w	1368w
$\nu_{asym}(CNC)$	1306s	1305s	1312s	1309s	1309s
$\nu_{sym}(CNC)$	1236vw	1237w	1239w	1241w	1241w
$\nu(CCl)$	768 mw	758mw	758m	760w	760w

Note: w, weak; m, medium; s, strong; vs, very strong; b, broad.
[a]Frequencies in cm^{-1}.

($\varepsilon = 5$ dm^3 M^{-1} cm^{-1}) and 693 nm ($\varepsilon = 15$ dm^3 M^{-1} cm^{-1}) may be attributed to $^4T_{1g}(F) \rightarrow {}^4A_{2g}(F)$ and $^4T_{1g}(F) \rightarrow {}^4T_{2g}(F)$ transitions, respectively, and a third band ($^4T_{1g}(F) \rightarrow {}^4T_{1g}(P)$ transition) is observed at 388 nm. The absorption spectra of **2** and **4** (Ni^{2+} complexes) showed three bands at 980 and 970 nm, 478 nm ($\varepsilon = 9$ dm^3 M^{-1} cm^{-1}) and 550 ($\varepsilon = 12$ dm^3 M^{-1} cm^{-1}), 391 and 390 nm assigned to the spin allowed transitions $^3A_{2g}(F) \rightarrow {}^3T_{2g}(F)$, $^3A_{2g}(F) \rightarrow {}^3T_{2g}(F)$ and $^3A_{2g}(F) \rightarrow {}^3T_{1g}(P)$, respectively (figure 9).

3.5. *Thermal analysis*

Complex **1** begins to decompose at 152 °C, from elimination of 0.5 M 3-pic with the endothermic step in DTA at 156 °C ($DTG_{max.}$ 113 and 224 °C). The experimental mass loss of 5.70% agrees with the calculated mass loss of 5.58%. In the second step, from 175 to 673 °C, the degradation of 1.5 M 3-pic and two dicl occurs with a mass loss of 85.30% (Calcd 87.61%; $DTG_{max.}$ 502 °C). The second step with one sharp and a medium exothermic DTA peaks at 257 and 503 °C results in formation of CoO [figure 10(a)].

The thermal decomposition of **2** occurs in three steps. The first step from 30 to 103 °C is assigned to loss of two waters with weight loss of 5.10% (calculated 4.12%, endothermic DTA peak at 95 °C). The second step from 103 to 257 °C corresponds to loss of two 3-pic, with the endothermic steps in the DTA at 118 and 221 °C. The experimental mass loss of 20.84% agrees with the calculated mass loss of 21.24% ($DTG_{max.}$ 113 and 224 °C). The third step from 242 to 597 °C corresponds to exothermic removal of two dicl with the exothermic DTA maxima at 480 and 535 °C. Good agreement between the experimental and calculated values was observed for the mass loss (exp. 68.50%; Calcd 67.96%; $DTG_{max.}$ 267 and 534 °C). The final thermal product is NiO, obtained at 597 °C [figure 10(b)].

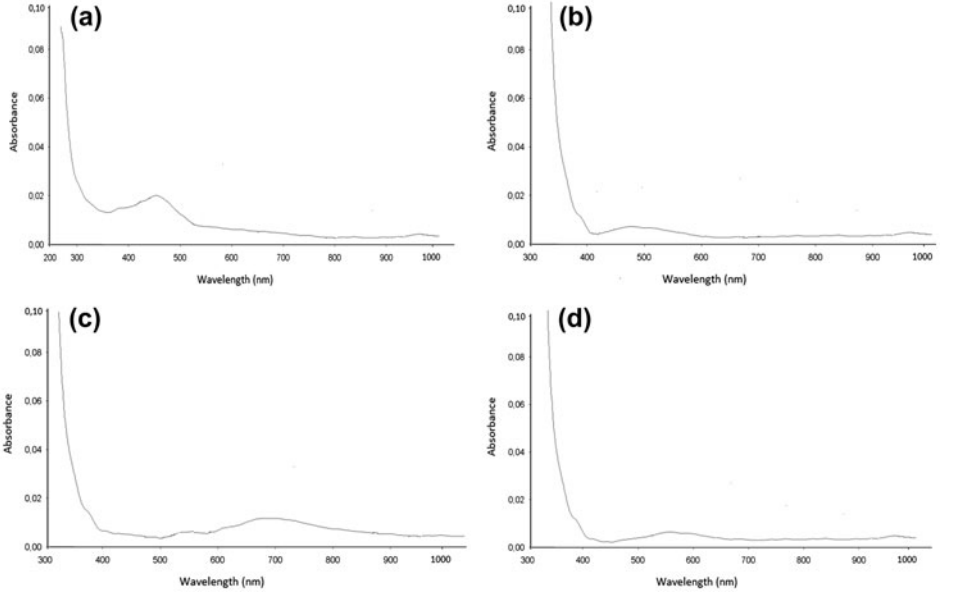

Figure 9. UV–Vis spectra of (a) **1**, (b) **2**, (c) **3**, and (d) **4**.

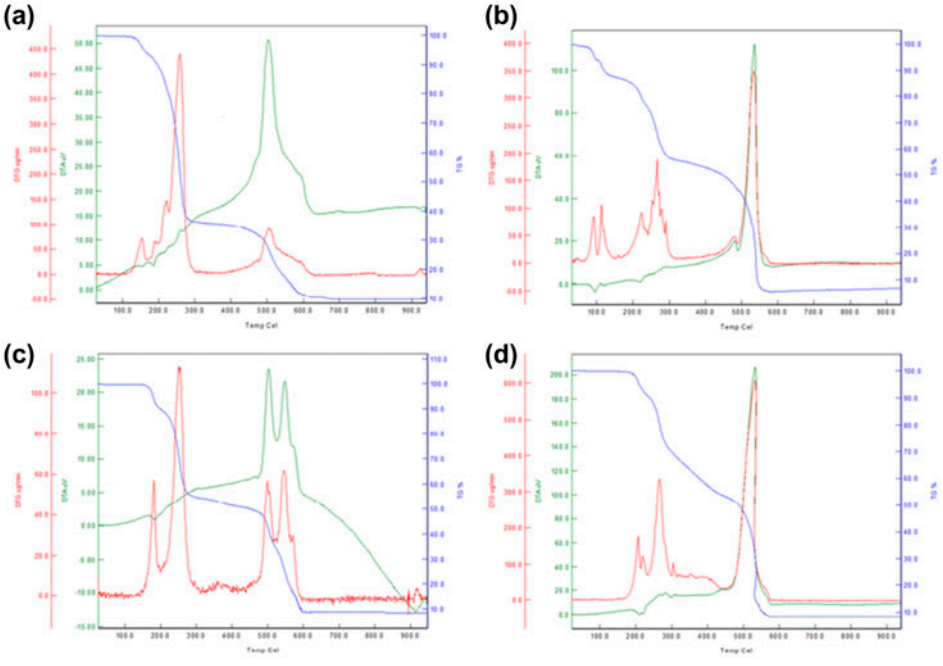

Figure 10. TG–DTA–DTG curves of (a) **1**, (b) **2**, (c) **3**, and (d) **4**.

The TG curve of **3** is shown in figure 10(c). The first endothermic stage (DTA at 183 °C) is related to removal of one 2-aepyr from 30 to 215 °C ($DTG_{max.}$ 180 °C, mass loss 13.50%, Calcd 13.01%). The second stage between 215 and 524 °C is related to release of one 2-aepyr and one dicl (DTA at 500 °C; $DTG_{max.}$ 252 and 502 °C; exp. 46.05; Calcd 46.74%). The third stage (DTA at 548 °C; DTG_{max} 548 °C) between 524 and 598 corresponds to loss of the remaining dicl (exp. 32.45%; calc. 33.74%). The final decomposition product is CoO.

The thermal behavior of **4** was followed to 900 °C in a static atmosphere of air. Complex **4** decomposes in three stages with the first stage at 30–248 °C corresponding to removal of one 2-aepyr with endothermic steps in the DTA at 208 °C (exp. mass loss 12.70%; Calcd 13.01%; $DTG_{max.}$ 207 and 218 °C). The second stage between 248 and 290 °C corresponds to loss of the remaining 2-aepyr (DTA at 283 °C; $DTG_{max.}$ 267 °C; exp. mass loss 13.05%; Calcd 13.01%). The following stage from 290 to 603 °C is related to release of two dicl ligands with DTA maxima at 301 and 534 °C ($DTG_{max.}$ 303 and 532 °C; exp. mass loss 66.35%; Calcd 67.48%). The final decomposition product is NiO [figure 10(d)].

3.6. *Purification and enzymatic activity of CA-I*

Purifications of CAs have been made so many times for the different organisms, and the effects of various chemicals were checked on these isoforms [10, 32–34]. CA-I was purified from human blood erythrocytes by affinity chromatography. The purified enzyme was characterized with a specific activity of 1210.46 EU/mg proteins, a yield of 60.00%, and a purification coefficient of 127.69 (table 5). The inhibitory effects of the neutral cobalt(II) and

Table 5. Inhibitory activities of synthesized complexes.

Complexes	I_{50} CA-I (mM)	K_i CA-I (mM)	Inhibition type
$Ni(dicl)_2(3\text{-pic})_2(H_2O)_2]$	0.223	0.188	Non-competitive
$[Ni(dicl)_2(2\text{-aepyr})_2]$	0.231	0.173	Non-competitive
$[Co(dicl)_2(2\text{-aepyr})_2]$	0.391	0.340	Non-competitive

Table 6. Purification of hCA-I.

Step	Activity (EU/mL)	Total volume (mL)	Protein (mg/mL)	Total protein (mg)	Total activity (EU)	Specific activity (EU/mg)	Recovery (%)	Purification (Fold)
Hemolysate	171.00	39.00	18.03	703.17	6669.00	9.48	100	1.00
hCA-I	462.00	8.65	0.38	3.29	3982.44	1210.46	60	127.69

*Mean value from at least three different measurements. Errors were in the range of ±3–5% of the obtained value (data not shown).

nickel(II) complexes with diclofenac in the presence of aromatic 3-picoline (3-pic) and non-aromatic 1-(2-aminoethyl)pyrrolidine (2-aepyr) were tested *in vitro*. The inhibitor concentrations that caused 50% inhibition (IC_{50}) were determined from % activity *versus* [Inhibitor] plots, and the K_i values were calculated from Lineweaver–Burk plots (table 6).

3.6.1. Investigation of inhibition type of CA. We prepared four chemical structures shown in figure 1 and evaluated their ability to inhibit hCA-I over a wide range of concentrations (0.001–1000 mM). Three of the four compounds inhibited hCA-I (table 6). Investigations show that many different chemicals and drugs inhibited hCA-I [32–34]. $[Ni(dicl)_2(3\text{-pic})_2(H_2O)_2]$, $[Co(dicl)_2(2\text{-aepyr})_2]$, and $[Ni(dicl)_2(2\text{-aepyr})_2]$ at low concentrations showed *in vitro* inhibitory effects on hCA-I. $[Ni(dicl)_2(2\text{-aepyr})_2]$ had the strongest inhibitory effects on hCA-I.

4. Conclusion

We have synthesized four new diclofenac cobalt(II) and nickel(II) complexes and studied their structural properties using FT-IR and UV–Vis spectroscopies, thermal analysis, and X-ray diffraction techniques. X-ray crystal structure analysis demonstrated that **1** and **3** have distorted octahedral geometry. Intramolecular N3–H3A···O2 and N4–H4A···O4 hydrogen bonds generate S(7) ring motives for **1**. Intramolecular N1–H1C···O2 and N3–H3D···O4 hydrogen bonds generate S(6) ring motives while N5–H5···O2 and N6–H6···O4 hydrogen bonds generate S(7) ring motives for **3**. Intra- and intermolecular hydrogen bonds stabilize this arrangement. **3** and **4** demonstrate higher thermal stability than **1** and **2**. $\Delta\nu$ indicates bidentate ($<200\ cm^{-1}$) coordination for **1**; monodentate ($>200\ cm^{-1}$) for **2**, **3**, and **4**. These compounds were checked for inhibition effects on hCA-I with **2**, **3**, and **4** showing non-competitive inhibition.

Supplementary material

Supplementary data CCDC-932105 and CCDC-932104 contain the supplementary crystallographic data for **1** and **3**, respectively. These data can be obtained free of charge via http://www.ccdc.cam.ac.uk/conts/retrieving.html, or from the Cambridge Crystallographic Data Center, 12 Union Road, Cambridge CB2 1EZ, UK; Fax: (+44) 1223 336 033; or E-mail: deposit@ccdc.cam.ac.uk.

Funding

This work was financially supported by the Erzincan University under the project no. 110205.

References

[1] C.P. Duffy, C.J. Elliott, R.A. O'Connor, M.M. Heenan, S. Coyle, I.M. Cleary, K. Kavanagh, S. Verhaegen, C.M. O'Loughlin, R. NicAmhlaoibh, M. Clynes. *Eur. J. Cancer*, **34**, 1250 (1998).
[2] J.E. Weder, C.T. Dillon, T.W. Hambley, B.J. Kennedy, P.A. Lay, J.R. Biffin, H.L. Regtop, N.M. Davies. *Coord. Chem. Rev.*, **232**, 95 (2002).
[3] S.B. Etcheverry, D.A. Barrio, A.M. Cortizo, P.A.M. Williams. *J. Inorg. Biochem.*, **88**, 94 (2002).
[4] M. Kyropoulou, C.P. Raptopoulou, V. Psycharis, G. Psomas. *Polyhedron*, **61**, 126 (2013).
[5] A. Quirinia, A. Viidik, S.J. Plast. *Reconstr. HandSurg.*, **31**, 213 (1997).
[6] J.N. Housby, C.M. Cahill, B. Chu, R. Prevelige, K. Bickford, M.A. Stevenson, S.K. Calderwood. *Cytokine*, **11**, 347 (1999).
[7] A. Beck, G. Krischak, T. Sorg, P. Augat, K. Farker, U. Merkel, L. Kinzl, L. Claes. *Arch. OrthopTraumaSurg.*, **123**, 327 (2003).
[8] M. Tunçay, S. Çaliş, H.S. Kaş, M.T. Ercan, I. Peksoy, A.A. Hincal. *Int. J. Pharm.*, **195**, 179 (2000).
[9] D. Kovala-Demertzi, D. Mentzafos, A. Terzis. *Polyhedron*, **12**, 1361 (1993).
[10] R.E. Tashian, D. Hewett-Emmett, N. Carter, N.C.H. Bergenhem. *Carbonic Anhydrase (CA)-related Proteins (CA-RPs), and Transmembrane Proteins with CA or CA-RP Domains*, In *The Carbonic Anhydrases*, W.R. Chegwidden, N. Carter, Y.H. Edwards (Eds), pp. 105–120, BirkhäuserVerlag, Basel (2000).
[11] W.R. Chegwidden, N.D. Carter. *EXS*, **90**, 13 (2000).
[12] A. Casini, A. Scozzafava, F. Mincione, L. Menabuoni, M. Starnotti, C.T. Supuran. *Bioorg. Med. Chem. Lett.*, **13**, 2867 (2003).
[13] I. Gülçin, S. Beydemir, M.E. Büyükokuroğlu. *Biol. Pharm. Bull.*, **27**, 613 (2004).
[14] D. Kovala-Demertzi, D. Mentzafos, A. Terzis. *Polyhedron*, **12**, 1361 (1993).
[15] J. Szejtli. *Cyclodextrins and Their Inclusion Complexes*, Akademia Kiodo, Budapest (1982).
[16] C.S.P. Sastry, A.R. Mohana Rao, T.H.V. Prasad. *Anal. Lett.*, **20**, 349 (1987).
[17] R.T. Sane, R.S. Samant, V.G. Nayak. *IndianDrugs*, **24**, 349 (1987).
[18] C.S.P. Sastry, A.S.R.P. Tipirneni, M.V. Suryanarayana. *Analyst*, **114**, 513 (1989).
[19] Y.K. Arrawal, V.P. Upadyay, S.K. Menon. *Indian J. Pharm. Sci.*, **50**, 58 (1988).
[20] B. Hennig, A.A. Steup, R. Benecke. *Pharmazie*, **42**, 861 (1987).
[21] W. Schneider, P.G. Degen. *J. Chromatogr.*, **217**, 263 (1981).
[22] D. Grandjean, J.C. Beolor, M.T. Quincon, E. Savel. *J. Pharm. Sci.*, **78**, 247 (1989).
[23] J. Godbillon, S. Gauron, J.P. Metayer. *J. Chromatogr.,* **338**, 151 (1985).
[24] S.A. Abdel Fattah, S.Z. El-Khateeb, S.A. AbdelRazeg, M.S. Tawakkol. *Spectrosc. Lett.*, **21**, 533 (1988).
[25] F. Dimiza, F. Perdih, V. Tangoulis, I. Turel, D.P. Kessissoglou, G. Psomas. *J. Inorg. Biochem.*, **105**, 476 (2011).
[26] D. Kovala-Demertzi, A. Theodorou, M.A. Demertzis, C.P. Raptopoulou, A. Terzis. *J. Inorg. Biochem.*, **65**, 151 (1997).
[27] C. Castellari, G. Feroci, S. Ottani. *Acta Crystallogr., Sect. C*, **55**, 907 (1999).
[28] N. Kourkoumelis, M.A. Demertzis, D. Kovala-Demertzi, A. Koutsodimou, A. Moukarika. *Spectrochim. Acta, Part A*, **60**, 2253 (2004).
[29] A.L. Speck. *PLATON, A Multipurpose Crystallographic Tool*, Utrecht University, the Netherlands (2001). http://www.cryst.chem.uu.nl/platon/.
[30] G.M. Sheldrick. *SHELXS97 and SHELXL97*, University of Göttingen, Germany (1997).
[31] Stoe & Cie. *X-Area (Version 1.18) and X-Red32 (Version 1.04)*, Stoe & Cie, Darmstadt, Germany (2002).
[32] M. Cankaya, M. Aktas, M. Kuzucu, İ. Gül, T.A. Coban. *J. Enzyme Inhib. Med. Chem.*, **27**, 641 (2012).

[33] T. Abdülkadir Coban, Ş. Beydemir, İ. Gulcin, D. Ekinci, A. Innocenti, D. Vullo, C.T. Supuran. *Bioorg. Med. Chem.*, **17**, 5791 (2009).
[34] S. Ayvaz, M. Çankaya, A. Atasever, A. Altuntas. *J. Enzyme Inhib. Med. Chem.*, **28**, 305 (2013).
[35] J.A. Verpoorte, S. Mehta, J.T. Edsall. *J. Biol. Chem.*, **242**, 4221 (1967).
[36] H. Lineweaver, D.J. Burk. *J. Am. Chem. Soc.*, **56**, 658 (1934).
[37] M.A. Bradford. *Anal. Biochem.*, **72**, 248 (1976).
[38] U.K. Laemmli. *Nature*, **227**, 680 (1970).
[39] S. Caglar, Z. Heren, O. Büyükgüngör. *J. Coord. Chem.*, **64**, 2706 (2011).
[40] S. Bajia, A. Mishra, R.J. Butcher, K.G. Ojha. *J. Coord. Chem.*, **63**, 4271 (2010).
[41] S.C. Bajia, J.E. Drake, M.E. Light, M. Nirwan, S.K. Pandey, R. Ratnani. *Polyhedron*, **28**, 85 (2009).
[42] Z. Xhu, J.H. Lin, Y.P. Yu, J. Xu, X.Z. You, S.X. Liu, C.C. Lin. *HuaxueXuebao*, **7**, 623 (1989).
[43] D. Wyrzykowski, E. Styczeń, Z. Warnke. *Transition Met. Chem.*, **31**, 860 (2006).
[44] J. Bernstein, R.E. Davis, L. Shimoni, N.L. Chang. *Angew. Chem. Int. Ed. Engl.*, **34**, 1555 (1995).
[45] L. Chen, X.-W. Wang, J.-Z. Chen, J.-H. Liu. *Z. Naturforsch.*, **62b**, 1271 (2007).
[46] K. Nakamoto. *Infrared and Raman Spectra of Inorganic and Coordination Compounds*, p. 230, Wiley, New York, NY (1986).